

ANALYSIS OF BLOCK-PRECONDITIONERS FOR MODELS OF COUPLED MAGMA/MANTLE DYNAMICS

SANDER RHEBERGEN*, GARTH N. WELLS†, RICHARD F. KATZ‡, AND ANDREW J. WATHEN§

Abstract. This article considers the iterative solution of a finite element discretisation of the magma dynamics equations. In simplified form, the magma dynamics equations share some features of the Stokes equations. We therefore formulate, analyse and numerically test a Elman, Silvester and Wathen-type block preconditioner for magma dynamics. We prove analytically and demonstrate numerically the optimality of the preconditioner. The presented analysis highlights the dependence of the preconditioner on parameters in the magma dynamics equations that can affect convergence of iterative linear solvers. The analysis is verified through a range of two- and three-dimensional numerical examples on unstructured grids, from simple illustrative problems through to large problems on subduction zone-like geometries. The computer code to reproduce all numerical examples is freely available as supporting material.

Key words. Magma dynamics, mantle dynamics, finite element method, preconditioners.

AMS subject classifications. 65F08, 76M10, 86A17, 86-08.

1. Introduction. The mantle of Earth extends from the bottom of the crust to the top of the iron core, some 3000 km below. Mantle rock, composed of silicate minerals, behaves as an elastic solid on the time scale of seismic waves but over geological time the mantle convects at high Rayleigh number as a creeping, viscous fluid [31]. This convective flow is the hidden engine for plate tectonics, giving rise to plate boundaries such as mid-ocean ridges (divergent) and subduction zones (convergent). Plate boundaries host the vast majority of terrestrial volcanism; their volcanoes are fed by magma extracted from below, where partial melting of mantle rock occurs (typically at depths less than ~ 100 km).

Partially molten regions of the mantle are of interest to geoscientists for their role in tectonic volcanism and in the chemical evolution of the Earth. The depth of these regions makes them inaccessible for direct observation, and hence studies of their dynamics have typically involved numerical simulation. Simulations are often based on a system of partial differential equations derived by McKenzie [27] and since elaborated and generalised by other authors [e.g., 10, 33, 34]. The equations describe two interpenetrating fluids of different density and vastly different viscosity: solid and molten rock (i.e., mantle and magma). The grains of the rock form a viscously deformable, permeable matrix through which magma can percolate. This is captured in the theory by a coupling of the Stokes equations for the mantle with Darcy's law for the magma. Although each phase is independently incompressible, the two-phase mixture allows for divergence or convergence of the solid matrix, locally increasing or decreasing the volume fraction of magma. This process is modulated by a compaction

*Mathematical Institute, University of Oxford, Andrew Wiles Building, Radcliffe Observatory Quarter, Woodstock Road, Oxford OX2 6GG, United Kingdom and Department of Earth Sciences, University of Oxford, South Parks Road, Oxford OX1 3AN, United Kingdom (sander.rhebergen@maths.ox.ac.uk).

†Department of Engineering, University of Cambridge, Trumpington Street, Cambridge CB2 1PZ, United Kingdom (gnw20@cam.ac.uk).

‡Department of Earth Sciences, University of Oxford, South Parks Road, Oxford OX1 3AN, United Kingdom (richard.katz@earth.ox.ac.uk).

§Mathematical Institute, University of Oxford, Andrew Wiles Building, Radcliffe Observatory Quarter, Woodstock Road, Oxford OX2 6GG, United Kingdom (andy.wathen@maths.ox.ac.uk).

viscosity, and gives rise to much of the interesting behaviour associated with coupled magma/mantle dynamics [35, 36, 20, 37].

The governing equations have been solved in a variety of contexts, from idealised studies of localisation and wave behaviour [e.g. 1, 8] to applied studies of plate-tectonic boundaries, especially mid-ocean ridges [e.g. 15, 18]. These studies have employed finite volume techniques on regular, Cartesian grids [e.g. 21]. Unlike mid-ocean ridges, subduction zones have a plate geometry that is awkward for Cartesian grids; it is, however, conveniently meshed with triangles or tetrahedra, which can also focus resolution where it is most needed [38]. Finite element simulations of pure mantle convection in subduction zones are common in the literature, but it remains a challenge to model two-phase, three-dimensional, magma/mantle dynamics of subduction, even though this is an area of active research [22, 39]. Such models require highly refined computational meshes, resulting in very large systems of algebraic equations. To solve these systems efficiently, iterative solvers together with effective preconditioning techniques are necessary. Although the governing equations are similar to those of Stokes flow, there has been no prior analysis of their discretisation and numerical solution by the finite element method.

The most computationally expensive step in modelling the partially molten mantle is typically the solution of a Stokes-like problem for the velocity of the solid matrix. To address this bottleneck in the context of large, unstructured grids for finite element discretisations, we describe, analyse, and test a preconditioner for the algebraic system resulting from the simplified McKenzie equations. The system of equations is similar to the Stokes problem, for which the Silvester–Wathen preconditioner [32] has been proven to be optimal, i.e., the iteration count of the iterative method is independent of the size of the algebraic system for a variety of discretisations of the Stokes equations (see also [26]). The key lies in finding a suitable approximation to the Schur complement of the block matrix resulting from the finite element discretisation. We follow this approach to prove and demonstrate numerically the optimality of the preconditioner for coupled magma/mantle dynamics problems. The analysis and numerical examples highlight some issues specific to magma/mantle dynamics simulations regarding the impact of model parameters on the solver performance. To the best of our knowledge, together with the work of Katz and Takei [19], we present the first three dimensional computations of the (simplified) McKenzie equations, and the first analysis of a preconditioner for this problem.

In this work we incorporate analysis, subduction zone-inspired examples, and software implementation. The analysis is confirmed by numerical examples that range from illustrative cases to large, representative models of subduction zones solved using parallel computers. The computer code to reproduce all presented examples is parallelised and is freely available under the Lesser GNU Public License (LGPL) as part of the supporting material [30]. The proposed preconditioning strategies have been implemented using libraries from the FEniCS Project [2, 24, 25, 28] and PETSc [5, 6, 7]. The FEniCS framework provides a high degree of mathematical abstraction, which permits the proposed methods to be implemented quickly, compactly and efficiently, with a close correspondence between the mathematical presentation in this paper and the computer implementation in the supporting material.

The outline of this article is as follows. In Section 2 we introduce the simplified McKenzie equations for coupled magma/mantle dynamics, followed by a finite element method for these equations in Section 3. A preconditioner analysis is conducted in Section 4 and its construction is discussed in Section 5. Through numerical simulations

in Section 6 we verify the analysis; conclusions are drawn in Section 7.

2. Partially molten magma dynamics. Let $\Omega \subset \mathbb{R}^d$ be a bounded domain with $2 \leq d \leq 3$. The McKenzie [27] model on Ω reads

$$(2.1) \quad \partial_t \phi - \nabla \cdot ((1 - \phi)\mathbf{u}) = 0,$$

$$(2.2) \quad -\nabla \cdot 2\eta\boldsymbol{\epsilon}(\mathbf{u}) + \nabla p_f = \nabla \left(\left(\zeta - \frac{2}{3}\eta \right) \nabla \cdot \mathbf{u} \right) - \bar{\rho}g\mathbf{e}_3,$$

$$(2.3) \quad \nabla \cdot \mathbf{u} = \nabla \cdot \frac{\kappa}{\mu} \nabla (p_f + \rho_f g z),$$

where ϕ is porosity, \mathbf{u} is the matrix velocity, $\boldsymbol{\epsilon}(\mathbf{u}) = (\nabla\mathbf{u} + (\nabla\mathbf{u})^T)/2$ is the strain rate tensor, κ is permeability, μ is the melt viscosity, η and ζ are the shear and bulk viscosity of the matrix, respectively, g is the constant acceleration due to gravity, \mathbf{e}_3 is the unit vector in the z -direction (i.e., $\mathbf{e}_3 = (0, 1)$ when $d = 2$ and $\mathbf{e}_3 = (0, 0, 1)$ when $d = 3$), p_f is the melt pressure, ρ_f and ρ_s are the constant melt and matrix densities, respectively, and $\bar{\rho} = \rho_f\phi + \rho_s(1 - \phi)$ is the phase-averaged density. Here we assume that μ , η and ζ are constants and that κ is a function of ϕ . The magma (fluid) velocity \mathbf{u}_f can be obtained from \mathbf{u} , ϕ and p_f through:

$$(2.4) \quad \mathbf{u}_f = \mathbf{u} - \frac{\kappa}{\phi\mu} \nabla (p_f + \rho_f g z).$$

It will be useful to decompose the melt pressure as $p_f = p - \rho_s g z$, where p is the dynamic pressure and $\rho_s g z$ the ‘lithostatic’ pressure. Equations (2.2), (2.3) and (2.4) may then be written as

$$(2.5) \quad -\nabla \cdot 2\eta\boldsymbol{\epsilon}(\mathbf{u}) + \nabla p = \nabla \left(\left(\zeta - \frac{2}{3}\eta \right) \nabla \cdot \mathbf{u} \right) + g\Delta\rho\phi\mathbf{e}_3,$$

$$(2.6) \quad \nabla \cdot \mathbf{u} = \nabla \cdot \frac{\kappa}{\mu} \nabla (p - \Delta\rho g z),$$

$$(2.7) \quad \mathbf{u}_f = \mathbf{u} - \frac{\kappa}{\phi\mu} \nabla (p - \Delta\rho g z),$$

where $\Delta\rho = \rho_s - \rho_f$. Constitutive relations are given by

$$(2.8) \quad \kappa = \kappa_0 \left(\frac{\phi}{\phi_0} \right)^n, \quad \zeta = r_\zeta \eta,$$

where ϕ_0 is the characteristic porosity, κ_0 the characteristic permeability, $n \geq 1$ is a dimensionless constant and r_ζ is the ratio between matrix bulk and shear viscosity. We non-dimensionalise (2.1), (2.5), (2.6) and (2.7) using

$$(2.9) \quad \mathbf{u} = u_0 \mathbf{u}', \quad \mathbf{x} = H \mathbf{x}', \quad t = (H/u_0)t', \quad \kappa = \kappa_0 \kappa', \quad p = \Delta\rho g H p',$$

where primed variables are non-dimensional, u_0 is the velocity scaling, given by

$$(2.10) \quad u_0 = \frac{\Delta\rho g H^2}{2\eta},$$

and H is a length scale. Dropping the prime notation, the McKenzie equations ((2.1), (2.5) and (2.6)), in non-dimensional form are given by

$$(2.11) \quad \partial_t \phi - \nabla \cdot ((1 - \phi)\mathbf{u}) = 0,$$

$$(2.12) \quad -\nabla \cdot \boldsymbol{\epsilon}(\mathbf{u}) + \nabla p = \nabla \left(\frac{1}{2} \left(r_\zeta - \frac{2}{3} \right) \nabla \cdot \mathbf{u} \right) + \phi \mathbf{e}_3,$$

$$(2.13) \quad \nabla \cdot \mathbf{u} = \frac{2R^2}{r_\zeta + 4/3} \nabla \cdot \left(\left(\frac{\phi}{\phi_0} \right)^n (\nabla p - \mathbf{e}_3) \right),$$

where $R = \delta/H$ with δ the compaction length defined as

$$(2.14) \quad \delta = \sqrt{\frac{(r_\zeta + 4/3)\kappa_0\eta}{\mu}},$$

and (2.7) becomes

$$(2.15) \quad \mathbf{u}_f = \mathbf{u} - \frac{2R^2}{r_\zeta + 4/3} \frac{1}{\phi} \left(\frac{\phi}{\phi_0} \right)^n (\nabla p - \mathbf{e}_3).$$

When solving the McKenzie model numerically for time-dependent simulations, (2.11) is usually decoupled from (2.12) and (2.13). Porosity is updated with (2.11) after which the velocity and pressure are determined by solving (2.12) and (2.13); iteration can be used to better capture the coupling. The most expensive part of this procedure is solving (2.12) and (2.13). In this work we study an optimal solver for equations (2.12) and (2.13) for a given porosity field. We remark that an alternative to decoupling (2.11) from (2.12) and (2.13) is to use a composable linear solver for the full system (2.11)-(2.13), see Brown et al. [12]. In this case, our optimal solver may be used as a preconditioner for part of this composable linear solver.

For the rest of this paper we replace $(r_\zeta - 2/3)/2$ by a constant α . Furthermore, we replace

$$(2.16) \quad \frac{R^2}{\alpha + 1} \left(\frac{\phi}{\phi_0} \right)^n$$

by a spatially variable function $k(\mathbf{x})$ (independent of α and ϕ) and we obtain the problem

$$(2.17a) \quad -\nabla \cdot \boldsymbol{\epsilon}(\mathbf{u}) + \nabla p = \nabla(\alpha \nabla \cdot \mathbf{u}) + \phi \mathbf{e}_3,$$

$$(2.17b) \quad \nabla \cdot \mathbf{u} = \nabla \cdot (k(\nabla p - \mathbf{e}_3)).$$

For coupled magma/mantle dynamics problems, α may range from $-1/3$ to approximately 1000. For this reason we will assume in this paper that $-1/3 \leq \alpha \leq 1000$. We also bound k : $0 \leq k_* \leq k(\mathbf{x}) \leq k^*$ for all $\mathbf{x} \in \Omega$. In the infinite-dimensional setting, we note that if $k(\mathbf{x}) = 0$ everywhere in Ω , the compaction stress $\nabla(\alpha \nabla \cdot \mathbf{u})$ vanishes as the velocity field is divergence free and (2.17) reduces to the Stokes equations. This will not generally be the case for a finite element formulation, as will be discussed in the following section.

On the boundary of the domain, $\partial\Omega$, we impose

$$(2.18) \quad \mathbf{u} = \mathbf{g},$$

$$(2.19) \quad -k(\nabla p - \mathbf{e}_3) \cdot \mathbf{n} = 0,$$

where $\mathbf{g} : \partial\Omega \rightarrow \mathbb{R}^d$ is given boundary data satisfying the compatibility condition

$$(2.20) \quad 0 = \int_{\partial\Omega} \mathbf{g} \cdot \mathbf{n} \, ds.$$

3. Finite element formulation. In this section we assume, without loss of generality, homogeneous boundary conditions on \mathbf{u} .

Let \mathcal{T}_h be a triangulation of Ω with associated finite element spaces $\mathbf{X}_h \subset (H_0^1(\Omega))^d$ and $M_h \subset H^1(\Omega) \cap L_0^2(\Omega)$. The finite element weak formulation for (2.17) and (2.18) is given by: find $\mathbf{u}_h, p_h \in \mathbf{X}_h \times M_h$ such that

$$(3.1) \quad \mathcal{B}(\mathbf{u}_h; p_h, \mathbf{v}; q) = \int_{\Omega} \phi \mathbf{e}_3 \cdot \mathbf{v} \, dx - \int_{\Omega} k \mathbf{e}_3 \cdot \nabla q \, dx \quad \forall \mathbf{v}, q \in \mathbf{X}_h \times M_h,$$

where

$$(3.2) \quad \mathcal{B}(\mathbf{u}; p, \mathbf{v}; q) = a(\mathbf{u}, \mathbf{v}) + b(p, \mathbf{v}) + b(q, \mathbf{u}) - c(p, q),$$

and

$$(3.3) \quad \begin{aligned} a(\mathbf{u}, \mathbf{v}) &= \int_{\Omega} \boldsymbol{\epsilon}(\mathbf{u}) : \boldsymbol{\epsilon}(\mathbf{v}) + \alpha(\nabla \cdot \mathbf{u})(\nabla \cdot \mathbf{v}) \, dx, \\ b(p, \mathbf{v}) &= - \int_{\Omega} p \nabla \cdot \mathbf{v} \, dx, \\ c(p, q) &= \int_{\Omega} k \nabla p \cdot \nabla q \, dx. \end{aligned}$$

PROPOSITION 3.1. *For $\alpha > -1$, there exists a $c_\alpha > 0$ such that*

$$(3.4) \quad a(\mathbf{v}, \mathbf{v}) \geq c_\alpha \|\mathbf{v}\|_1^2 \quad \forall \mathbf{v} \in (H_0^1(\Omega))^d.$$

Proof. The proposition follows from

$$(3.5) \quad \|\nabla \cdot \mathbf{v}\|^2 \leq \|\boldsymbol{\epsilon}(\mathbf{v})\|^2 \leq \|\nabla \mathbf{v}\|^2 \quad \forall \mathbf{v} \in (H_0^1(\Omega))^d,$$

(see Ref. [16, Eq. (3.4)]) and the application of Korn's inequality. \square

We will consider finite elements that are inf-sup stable [11] in the degenerate limit of $k = 0$, i.e., $a(\mathbf{u}, \mathbf{v})$ is coercive (see Proposition 3.1), $c(p, p) \geq 0 \, \forall p \in M_h$ and for which there exists a constant $c_1 > 0$ independent of h such that

$$(3.6) \quad \max_{\mathbf{v}_h \in \mathbf{X}_h} \frac{b(q_h, \mathbf{v}_h)}{\|\nabla \mathbf{v}_h\|} \geq c_1 \|q_h\| \quad \forall q_h \in M_h.$$

In particular, we will use Taylor–Hood (P^2 – P^1) finite elements on simplices. We note that while in the infinite-dimensional setting the Stokes equations are recovered from (2.17) when $k = 0$, this is not generally the case for the discrete weak formulation in (3.1) when $\alpha \neq 0$. Obtaining the Stokes limit in the finite element setting when $\alpha \neq 0$ requires the non-trivial property that the divergence of functions in \mathbf{X}_h lie in the pressure space M_h . This is not the case for Taylor–Hood finite elements.

The discrete system (3.1) can be written in block matrix form as

$$(3.7) \quad \begin{bmatrix} A & B^T \\ B & -C_k \end{bmatrix} \begin{bmatrix} u \\ p \end{bmatrix} = \begin{bmatrix} f \\ g \end{bmatrix},$$

where $u \in \mathbb{R}^{n_u}$ and $p \in N^{n_p} = \{q \in \mathbb{R}^{n_p} | q \neq 1\}$ are, respectively, the vectors of the discrete velocity and pressure variables with respect to appropriate bases for \mathbf{X}_h and M_h . The space N^{n_p} satisfies the zero mean pressure condition.

For later convenience, we define the negative of the ‘pressure’ Schur complement S :

$$(3.8) \quad S = BA^{-1}B^T + C_k,$$

and the scalar pressure mass matrix Q such that

$$(3.9) \quad \|q_h\|^2 = \langle Qq, q \rangle,$$

for $q_h \in M_h$ and where $q \in \mathbb{R}^{n_p}$ is the vector of the coefficients associated with the pressure basis and $\langle \cdot, \cdot \rangle$ denotes the standard Euclidean scalar product.

The differences between the matrix formulation of the magma/mantle equations (2.17) and the Stokes equations lie in the matrices A and C_k . In the case of the magma/mantle dynamics, A includes the discretisation of compaction stresses: a ‘grad-div’ term weighted by the factor α . Such ‘grad-div’ terms are known to be problematic in the context of multigrid methods as the modes associated with lowest eigenvalues are not well represented on a coarse grid [3]. There have been a number of investigations into this issue for $H(\text{div})$ finite element problems, e.g. [4, 23]. The second matrix which differs from the Stokes discretisation is C_k . For sufficiently large k , this term provides Laplace-type pressure stabilisation for elements that would otherwise be unstable for the Stokes problem.

4. Optimal block diagonal preconditioners. To model three-dimensional magma/mantle dynamics of subduction, efficient iterative solvers together with preconditioning techniques are needed to solve the resulting algebraic systems of equations. The goal of this section is to introduce and prove optimality of a class of block diagonal preconditioners for (3.7).

To prove optimality of a block preconditioner for the McKenzie problem, we first present a number of supporting results.

PROPOSITION 4.1. *The bilinear form c in (3.3) satisfies*

$$(4.1) \quad c(q, q) \geq k_* \|\nabla q\|^2 \quad \forall q \in M^h.$$

Proof. This follows directly from

$$(4.2) \quad c(q, q) = \left\| k^{1/2} \nabla q \right\|^2 \geq \left\| k_*^{1/2} \nabla q \right\|^2.$$

□

LEMMA 4.2. *For the matrices A , B and C_k given in (3.7), the pressure Schur complement S in (3.8) and the pressure mass matrix Q in (3.9), for an inf-sup stable formulation satisfying (3.6), the following bounds hold*

$$(4.3) \quad 0 < c_q \leq \frac{\langle Sq, q \rangle}{\langle (Q + C_k)q, q \rangle} \leq c^q, \quad \forall q \in N^{n_p},$$

where c^q is given by

$$(4.4) \quad c^q = \begin{cases} 1/(1 - |\alpha|) & \text{if } -1/3 \leq \alpha < 0, \\ 1 & \text{if } \alpha \geq 0, \end{cases}$$

and c_q by

$$(4.5) \quad c_q = \min \left(\frac{c_1^2 + c_P k_* (1 + |\alpha|)}{(1 + |\alpha|)(1 + c_P k_*)}, 1 \right),$$

where c_1 is the inf-sup constant and c_P the Poincaré constant.

Proof. Since A is symmetric and positive definite, and from the definition of S

$$(4.6) \quad \begin{aligned} \langle Sq, q \rangle &= \langle A^{-1} B^T q, B^T q \rangle + \langle C_k q, q \rangle \\ &= \sup_{v \in \mathbb{R}^{n_u}} \frac{\langle v, B^T q \rangle^2}{\langle Av, v \rangle} + \langle C_k q, q \rangle, \end{aligned}$$

for all $q \in N^{np}$. From the definition of matrices A, B, C_k and Q it then follows that

$$(4.7) \quad \langle Sq, q \rangle = \sup_{\mathbf{v}_h \in \mathbf{X}_h} \frac{(q_h, \nabla \cdot \mathbf{v}_h)^2}{\|\boldsymbol{\epsilon}(\mathbf{v}_h)\|^2 + \alpha \|\nabla \cdot \mathbf{v}_h\|^2} + (k \nabla q_h, \nabla q_h).$$

Using (3.5) and the Cauchy–Schwarz inequality,

$$(4.8) \quad (q_h, \nabla \cdot \mathbf{v}_h)^2 \leq \|q_h\|^2 \|\boldsymbol{\epsilon}(\mathbf{v}_h)\|^2.$$

For $-1/3 \leq \alpha < 0$,

$$(4.9) \quad \begin{aligned} \|\boldsymbol{\epsilon}(\mathbf{v}_h)\|^2 &= \frac{1}{1 + \alpha} \left(\|\boldsymbol{\epsilon}(\mathbf{v}_h)\|^2 + \alpha \|\boldsymbol{\epsilon}(\mathbf{v}_h)\|^2 \right) \\ &\leq \frac{1}{1 + \alpha} \left(\|\boldsymbol{\epsilon}(\mathbf{v}_h)\|^2 + \alpha \|\nabla \cdot \mathbf{v}_h\|^2 \right), \end{aligned}$$

and for $\alpha \geq 0$,

$$(4.10) \quad \|\boldsymbol{\epsilon}(\mathbf{v}_h)\|^2 \leq \|\boldsymbol{\epsilon}(\mathbf{v}_h)\|^2 + \alpha \|\nabla \cdot \mathbf{v}_h\|^2.$$

Hence,

$$(4.11) \quad (q_h, \nabla \cdot \mathbf{v}_h)^2 \leq c^q \|q_h\|^2 \left(\|\boldsymbol{\epsilon}(\mathbf{v}_h)\|^2 + \alpha \|\nabla \cdot \mathbf{v}_h\|^2 \right),$$

where

$$(4.12) \quad c^q = \begin{cases} 1/(1 - |\alpha|) & \text{if } -1/3 \leq \alpha < 0, \\ 1 & \text{if } \alpha \geq 0. \end{cases}$$

Combining (4.7) and (4.11),

$$(4.13) \quad \langle Sq, q \rangle \leq c^q \|q_h\|^2 + (k \nabla q_h, \nabla q_h) = c^q \langle Qq, q \rangle + \langle C_k q, q \rangle \leq c^q \langle (Q + C_k)q, q \rangle.$$

This proves the upper bound in (4.3).

Next we determine the lower bound. Using (3.5) and the inf-sup condition (3.6),

$$(4.14) \quad \begin{aligned} \max_{\mathbf{v}_h \in \mathbf{X}_h} \frac{(q_h, \nabla \cdot \mathbf{v}_h)^2}{\|\boldsymbol{\epsilon}(\mathbf{v}_h)\|^2 + \alpha \|\nabla \cdot \mathbf{v}_h\|^2} &\geq \max_{\mathbf{v}_h \in \mathbf{X}_h} \frac{(q_h, \nabla \cdot \mathbf{v}_h)^2}{(1 + |\alpha|) \|\nabla \mathbf{v}_h\|^2} \\ &\geq \frac{c_1^2}{1 + |\alpha|} \|q_h\|^2, \end{aligned}$$

which leads to

$$(4.15) \quad \langle Sq, q \rangle \geq \frac{c_1^2}{1 + |\alpha|} \langle Qq, q \rangle + \langle C_k q, q \rangle.$$

Using Proposition 4.1 and the Poincaré inequality,

$$(4.16) \quad \begin{aligned} \langle C_k q, q \rangle &= (1 - \xi)c(q_h, q_h) + \xi \left\| k^{1/2} \nabla q_h \right\|^2 \\ &\geq (1 - \xi)c(q_h, q_h) + \xi c_P k_* \|q_h\|^2 \\ &= (1 - \xi) \langle C_k q, q \rangle + \xi c_P k_* \langle Qq, q \rangle, \end{aligned}$$

for any $\xi \in [0, 1]$. Combining (4.15) and (4.16),

$$(4.17) \quad \langle Sq, q \rangle \geq \left(\frac{c_1^2}{1 + |\alpha|} + \xi c_P k_* \right) \langle Qq, q \rangle + (1 - \xi) \langle C_k q, q \rangle,$$

and setting $\xi = (1 - c_1^2/(1 + |\alpha|))/(1 + c_P k_*)$ in the case that $c_1^2/(1 + |\alpha|) \leq 1$, and otherwise setting $\xi = 0$,

$$(4.18) \quad \langle Sq, q \rangle \geq \min \left(\frac{c_1^2 + c_P k_* (1 + |\alpha|)}{(1 + |\alpha|)(1 + c_P k_*)}, 1 \right) \langle (Q + C_k)q, q \rangle,$$

from which c_q is deduced. \square

For the discretisation of the Stokes equations, it was shown that the pressure mass-matrix is spectrally equivalent to the Schur complement [32]. This is recovered from Lemma 4.2 when $k = 0$ everywhere and $\alpha = 0$.

LEMMA 4.3. *For the matrices A , B and C_k in (3.7), S in (3.8) and the pressure mass matrix Q in (3.9), if the inf-sup condition in (3.6) is satisfied, then*

$$(4.19) \quad \frac{\langle (B^T(Q + C_k)^{-1}Bv, v) \rangle}{\langle Av, v \rangle} \leq c^q \quad \forall v \in \mathbb{R}^{n_u},$$

where c^q is the constant from in (4.4).

Proof. From Lemma 4.2, symmetry of A and positive semi-definiteness of C ,

$$(4.20) \quad \frac{q^T B A^{-1} B^T q}{q^T (Q + C_k) q} \leq \frac{q^T (B A^{-1} B^T + C_k) q}{q^T (Q + C_k) q} \leq c^q \quad \forall q \in N^{n_p}.$$

Inserting $q \leftarrow (Q + C_k)^{1/2} q$,

$$(4.21) \quad \frac{q^T (Q + C_k)^{-1/2} B A^{-1} B^T (Q + C_k)^{-1/2} q}{q^T q} \leq c^q \quad \forall q \in N^{n_p}.$$

Defining $H = (Q + C_k)^{-1/2} B A^{-1} B^T (Q + C_k)^{-1/2}$ and denoting the maximum eigenvalue of H by λ_{\max} and associated eigenvector x , since H is symmetric it follows that $\lambda_{\max} \geq v^T H v / (v^T v) \forall v \in \mathbb{R}^n$ and $\lambda_{\max} = x^T H x / (x^T x)$. Hence, $\lambda_{\max} \leq c^q$, and

$$(4.22) \quad (Q + C_k)^{-1/2} B A^{-1} B^T (Q + C_k)^{-1/2} x = \lambda_{\max} x,$$

and pre-multiplying both sides by $A^{-1/2} B^T (Q + C_k)^{-1/2}$,

$$(4.23) \quad \begin{aligned} A^{-1/2} B^T (Q + C_k)^{-1/2} (Q + C_k)^{-1/2} B A^{-1/2} A^{-1/2} B^T (Q + C_k)^{-1/2} x \\ = \lambda_{\max} A^{-1/2} B^T (Q + C_k)^{-1/2} x. \end{aligned}$$

Letting $v = A^{-1/2}B^T(Q + C_k)^{-1/2}x$, the above becomes

$$(4.24) \quad A^{-1/2}B^T(Q + C_k)^{-1}BA^{-1/2}v = \lambda_{\max}v,$$

and it follows from $\lambda_{\max} \leq c^q$ that

$$(4.25) \quad \frac{v^T A^{-1/2}B^T(Q + C_k)^{-1}BA^{-1/2}v}{v^T v} \leq c^q \quad \forall v \in \mathbb{R}^{n_u},$$

or, taking $v \leftarrow A^{-1/2}v$,

$$(4.26) \quad \frac{v^T B^T(Q + C_k)^{-1}Bv}{v^T Av} \leq c^q \quad \forall v \in \mathbb{R}^{n_u},$$

and the Lemma follows. \square

We now consider diagonal block preconditioners for (3.7) of the form

$$(4.27) \quad \mathcal{P} = \begin{bmatrix} P & 0 \\ 0 & T \end{bmatrix}, \quad P \in \mathbb{R}^{n_u \times n_u}, \quad T \in \mathbb{R}^{n_p \times n_p}.$$

We assume that P and T are symmetric and positive-definite, and that they satisfy

$$(4.28) \quad \delta_{AP} \leq \frac{\langle Av, v \rangle}{\langle Pv, v \rangle} \leq \delta^{AP} \quad \forall v \in \mathbb{R}^{n_u}, \quad \delta_{QT} \leq \frac{\langle (Q + C_k)q, q \rangle}{\langle Tq, q \rangle} \leq \delta^{QT} \quad \forall q \in \mathbb{R}^{n_p},$$

where δ_{AP} , δ^{AP} , δ_{QT} and δ^{QT} are independent of h , but may depend on model parameters.

The discrete system in (3.7) is indefinite, and hence has both positive and negative eigenvalues. The speed of convergence of the MINRES Krylov method for the preconditioned system

$$(4.29) \quad \begin{bmatrix} P & 0 \\ 0 & T \end{bmatrix}^{-1} \begin{bmatrix} A & B^T \\ B & -C_k \end{bmatrix} \begin{bmatrix} u \\ p \end{bmatrix} = \begin{bmatrix} P & 0 \\ 0 & T \end{bmatrix}^{-1} \begin{bmatrix} f \\ g \end{bmatrix},$$

depends on how tightly the positive and negative eigenvalues of the generalised eigenvalue problem

$$(4.30) \quad \begin{bmatrix} A & B^T \\ B & -C_k \end{bmatrix} \begin{bmatrix} v \\ q \end{bmatrix} = \lambda \begin{bmatrix} P & 0 \\ 0 & T \end{bmatrix} \begin{bmatrix} v \\ q \end{bmatrix},$$

are clustered [13, Section 6.2]. Our aim now is to develop bounds on the eigenvalues in (4.30) that are independent of the mesh parameter h .

THEOREM 4.4. *Let c_q and c^q be the constants in Lemma 4.2, and the matrices A , B and C_k be those given in (3.7), S be the pressure Schur complement in (3.8) and Q the pressure mass matrix in (3.9). If P and T satisfy (4.28), all eigenvalues $\lambda < 0$ of (4.30) satisfy*

$$(4.31) \quad -c^q \delta^{QT} \leq \lambda \leq \frac{1}{2} \left(\delta_{AP} - \sqrt{\delta_{AP}^2 + 4c_q \delta_{QT} \delta_{AP}} \right),$$

and eigenvalues $\lambda > 0$ of (4.30) satisfy

$$(4.32) \quad \delta_{AP} \leq \lambda \leq \delta^{AP} + c^q \delta^{QT}.$$

Proof. Lemmas 4.2 and 4.3 provide the bounds

$$(4.33) \quad c_q \leq \frac{\langle Sq, q \rangle}{\langle (Q + C_k)q, q \rangle} \leq c^q, \quad \frac{\langle (B^T(Q + C_k)^{-1}Bv, v) \rangle}{\langle Av, v \rangle} \leq c^q,$$

for all $q \in N^{n_p}$ and $\forall v \in \mathbb{R}^{n_u}$. Using these bounds together with the bounds given in (4.28), the result follows directly by following the proof of Theorem 6.6 in Elman et al. [13], or more generally Pestana and Wathen [29]. \square

The main result of this section, Theorem 4.4, states that the eigenvalues of the generalised eigenvalue problem (4.30) are independent of the problem size. From Theorem 4.4 we see that

$$(4.34) \quad \lambda \in \left[-c^q \delta^{QT}, \frac{1}{2} \left(\delta_{AP} - \sqrt{\delta_{AP}^2 + 4c_q \delta_{QT} \delta_{AP}} \right) \right] \cup \left[\delta_{AP}, \delta^{AP} + c^q \delta^{QT} \right],$$

in which all constants are independent of the problem size (independent of h). This tells us that if we can find a P and T that are spectrally equivalent to A and $Q + C_k$, respectively, then an iterative method with preconditioner (4.27) will be optimal for (3.7).

The interval in (4.34) shows the dependence of the eigenvalues on α and k . The upper and lower bounds on the positive eigenvalues are well behaved, as is the lower bound on the negative eigenvalues, for all α and k . It is only when $c_q \ll 1$ that the upper bound on the negative eigenvalues tends to zero. If this is the case, the rate of convergence of the iterative method may slow. From (4.5), we see that $c_q \ll 1$ only if $\alpha \gg 1$ and, at the same time, $k_* \ll 1$.

5. Preconditioner construction. Implementation of the proposed preconditioner requires the provision of symmetric, positive definite matrices P and T that satisfy (4.28). Obvious candidates are $P = A$ and $T = Q + C_k$, with a direct solver used to compute the action of P^{-1} and T^{-1} . We will use this for small problems in the following section to study the performance of the block preconditioning; the application of a direct solver is not practical, however, when P and T are large, in which case we advocate the use of multigrid approximations of the inverse.

To provide more general guidance, we first reproduce the following Lemma from Elman et al. [13, Lemma 6.2].

LEMMA 5.1. *If u is the solution to the system $Au = f$ and*

$$(5.1) \quad u_{i+1} = (I - P^{-1}A)u_i + P^{-1}f,$$

then if the iteration error satisfies $\langle A(u - u_{i+1}), u - u_{i+1} \rangle \leq \rho \langle A(u - u_i), u - u_i \rangle$, with $\rho < 1$,

$$(5.2) \quad 1 - \rho \leq \frac{\langle Av, v \rangle}{\langle Pv, v \rangle} \leq 1 + \rho \quad \forall v.$$

Proof. See Elman et al. [13, proof of Lemma 6.2]. \square

Lemma 5.1 implies that a solver that is optimal for $Au = f$ will satisfy (4.28), and is therefore a candidate for P , and likewise for T . The obvious candidates for P and T are multigrid preconditioners applied to A and $Q + C_k$, respectively. However, as we will show by example in Section 6, as α increases, and therefore the compaction stresses (a ‘grad-div’ term) become more important, multigrid for P becomes less effective as a preconditioner. More effective treatment of the large α case is the subject of ongoing investigations.

6. Numerical simulations. In this section we verify the analysis results through numerical examples. In all test cases we use P^2 - P^1 Taylor–Hood finite elements on simplices. The numerical examples deliberately address points of practical interest such as spatial variations in the parameter k , a wide range of values for α and large problem sizes on unstructured grids of subduction zone-like geometries.

We consider two preconditioners. For the first, we take $P = A$ and $T = Q + C_k$ in (4.27) and apply a direct solver to compute the action of the inverses. This preconditioner will be referred to as the ‘LU’ preconditioner. For the second, we use $P^{-1} = A^{\text{AMG}}$ and $T^{-1} = (Q + C_k)^{\text{AMG}}$, where we use $(\cdot)^{\text{AMG}}$ to denote the use of algebraic multigrid to approximate the inverse of (\cdot) . This preconditioner will be referred to as the ‘AMG’ preconditioner. The LU preconditioner is introduced as a reference preconditioner to which the AMG preconditioner can be compared. The LU preconditioner is not suitable for large scale problems. Note that we never construct the inverse of P or T , but that we just use the action of the inverse.

All tests use the MINRES method, and the solver is terminated once a relative true residual of 10^{-8} is reached. For multigrid approximations of P^{-1} , smoothed aggregation algebraic multigrid is used via the library ML [14]. For multigrid approximations of T^{-1} , classical algebraic multigrid is used via the library BoomerAMG [17]. Unless otherwise stated, we use multigrid V-cycles, with two applications of Chebyshev with Jacobi smoothing on each level (pre and post) in the case of smoothed aggregation, and symmetric Gauss–Seidel for the classical algebraic multigrid. The computer code is developed using the finite element library DOLFIN [24], with block preconditioner support from PETSc [12] to construct the preconditioners. The computer code to reproduce all examples is freely available in the supporting material [30].

6.1. Verification of optimality. In this test case we verify optimality of the block preconditioned MINRES scheme by observing the convergence of the solver for varying h , α , k^* and k_* . We solve (2.17) and (2.18) on the unit square domain $\Omega = (0, 1)^2$ using a regular mesh of triangular cells. For the permeability, we consider

$$(6.1) \quad k = \frac{k^* - k_*}{4 \tanh(5)} (\tanh(10x - 5) + \tanh(10z - 5) + \frac{2(k^* - k_*) - 2 \tanh(5)(k_* + k^*)}{k_* - k^*} + 2).$$

We ignore body forces but add a source term \mathbf{f} to the right hand side of (2.17a). The Dirichlet boundary condition \mathbf{g} and the source term \mathbf{f} are constructed such that the exact solution pressure p and velocity \mathbf{u} are:

$$(6.2) \quad p = -\cos(4\pi x) \cos(2\pi z),$$

$$(6.3) \quad u_x = k \partial_x p + \sin(\pi x) \sin(2\pi z) + 2,$$

$$(6.4) \quad u_z = k \partial_z p + \frac{1}{2} \cos(\pi x) \cos(2\pi z) + 2.$$

Table 6.1 shows the number of iterations the MINRES method required to converge using the LU and AMG preconditioners with $k_* = 0.5$ and $k^* = 1.5$, when varying α from $-1/3$ to 1000. We clearly see that the LU preconditioner is optimal (the iteration count is independent of the problem size), as predicted by the analysis (see Theorem 4.4). Using the AMG preconditioner, there is a very slight dependence on the problem size. The results in Table 6.1 indicate that the LU preconditioner

Table 6.1: Number of iterations for the LU and AMG preconditioned MINRES for the unit square test with different levels of mesh refinement and for different values of α . The number of degrees-of-freedom is denoted by N . For the $\alpha = 1000$ case, four applications of a Chebyshev smoother, with one symmetric Gauss-Seidel iteration for each application, was used.

N	$\alpha = -\frac{1}{3}$		$\alpha = 0$		$\alpha = 1$		$\alpha = 10$		$\alpha = 1000$	
	LU	AMG	LU	AMG	LU	AMG	LU	AMG	LU	AMG*
9,539	9	29	9	30	9	35	8	67	7	202
37,507	9	33	9	36	9	40	8	80	6	283
148,739	8	39	8	40	9	47	7	96	6	366
592,387	8	42	8	44	7	52	7	106	6	432

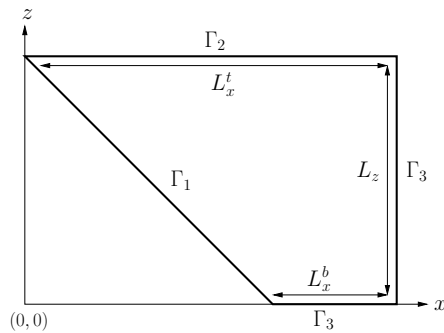


Fig. 6.1: Description of the wedge geometry for a two-dimensional subduction zone.

is uniform with respect to α . Theorem 4.4 indicates a possible dependence on α through the constant c_q . However, for α sufficiently small or sufficiently large, the dependence of c_q on α becomes negligible, and α has only a small impact on the iteration count. The AMG preconditioner, on the other hand, shows a strong dependence on α . The issue with the ‘grad-div’ for multigrid solvers was discussed in Section 3, and is manifest in Table 6.1. It has been observed in tests that the effectiveness of a multigrid preconditioned solver for the operator A deteriorates with increasing α . This is manifest in an increasing ρ in (5.2) for increasing α .

Results for the case of large spatial variations in permeability k are presented in Tables 6.2 and 6.3 for the cases $\alpha = 1$ and $\alpha = 100$, respectively. A dependence of the iteration count on the permeability is observed. The smaller k^* , the larger the iteration counts for both the AMG and the LU preconditioners. We also observe that for a given k^* there is little influence of k_* on the iteration count. Comparing the results in Tables 6.2 and 6.3 we see that the LU preconditioner shows no dependence on α . For the AMG preconditioner the iteration count increases as α increases from 1 to 100.

6.2. A magma dynamics problem in two dimensions. In this test case we solve (2.17) and (2.18) on a domain Ω , depicted in Figure 6.1, using unstructured meshes with triangular cells. We take $L_x^t = 1.5$, $L_x^b = 0.5$ and $L_z = 1$. We set the permeability as $k = 0.9(1 + \tanh(-2r))$ with $r = \sqrt{x^2 + z^2}$ and the porosity $\phi = 0.01$.

Table 6.2: Number of iterations to reach a relative tolerance of 10^{-8} using preconditioned MINRES for the unit square test with varying levels of mesh refinement and varying (k_*, k^*) pairs for $\alpha = 1$. The number of degrees of freedom is denoted by N .

$k^* = 10^{-4}$	$k_* = 0$		$k_* = 10^{-8}$		$k_* = 10^{-6}$		$k_* = 5 \cdot 10^{-5}$	
N	LU	AMG	LU	AMG	LU	AMG	LU	AMG
9,539	32	88	32	88	32	88	32	80
37,507	35	108	35	108	35	108	35	97
148,739	38	130	37	130	38	127	33	111
592,387	36	143	36	143	35	135	33	122
$k^* = 1$	$k_* = 0$		$k_* = 0.1$		$k_* = 0.5$		$k_* = 0.9$	
N	LU	AMG	LU	AMG	LU	AMG	LU	AMG
9,539	27	67	10	37	9	36	9	36
37,507	28	78	10	44	9	42	9	42
148,739	28	93	10	50	9	48	7	47
592,387	27	101	10	54	9	52	7	52
$k^* = 1000$	$k_* = 0$		$k_* = 1$		$k_* = 10$		$k_* = 100$	
N	LU	AMG	LU	AMG	LU	AMG	LU	AMG
9,539	3	24	3	26	3	24	3	24
37,507	3	27	3	27	3	27	3	30
148,739	3	34	3	33	3	34	3	33
592,387	3	37	3	37	3	37	3	40
$k^* = 10^8$	$k_* = 0$		$k_* = 1$		$k_* = 10^3$		$k_* = 10^6$	
N	LU	AMG	LU	AMG	LU	AMG	LU	AMG
9,539	1	15	1	15	1	15	1	15
37,507	2	18	2	18	2	18	2	18
148,739	2	21	2	21	2	21	2	21
592,387	2	21	2	21	2	21	2	21

We consider two test cases for this geometry. The first test problem we denote as the *analytical corner flow* test problem and the second as the *traction-free* test problem. In both problems we prescribe the following conditions: $\mathbf{u} = \mathbf{u}_{\text{slab}} = (1, -1)/\sqrt{2}$ on Γ_1 , $\mathbf{u} = \mathbf{0}$ on Γ_2 and $-k(\nabla p - \mathbf{e}_3) \cdot \mathbf{n} = 0$ on $\partial\Omega$.

6.2.1. Analytic corner flow. For the analytical corner flow problem we prescribe $\mathbf{u} = \mathbf{u}_{\text{corner}} = (u_x, u_z)$ on Γ_3 , which is the analytic expression for corner-flow [9, Section 4.8]. The corner-flow velocity components u_x and u_z are given by

$$(6.5) \quad u_x = \cos(\theta)u_r + \sin(\theta)u_\theta, \quad u_z = -\sin(\theta)u_r + \cos(\theta)u_\theta,$$

where $\theta = -\arctan(\tilde{z}/x)$, $\tilde{z} = z - 1$ and

$$(6.6) \quad u_r = C\theta \sin(\theta) + D(\sin(\theta) + \theta \cos(\theta)), \quad u_\theta = C(\sin(\theta) - \theta \cos(\theta)) + D\theta \sin(\theta),$$

with

$$(6.7) \quad C = \frac{\beta \sin(\beta)}{\beta^2 - \sin^2(\beta)}, \quad D = \frac{\beta \cos(\beta) - \sin(\beta)}{\beta^2 - \sin^2(\beta)}.$$

Table 6.3: Number of iterations to reach a relative tolerance of 10^{-8} using preconditioned MINRES for the unit square test with varying levels of mesh refinement and varying (k_*, k^*) pairs for $\alpha = 100$. The number of degrees of freedom is denoted by N .

$k^* = 10^{-4}$ N	$k_* = 0$		$k_* = 10^{-8}$		$k_* = 10^{-6}$		$k_* = 5 \cdot 10^{-5}$	
	LU	AMG	LU	AMG	LU	AMG	LU	AMG
9,539	67	1605	67	1598	66	1557	58	1385
37,507	75	1922	75	1922	71	1909	62	1730
148,739	76	2179	76	2177	72	2146	59	1972
592,387	73	2356	73	2356	68	2311	59	2156
$k^* = 1$ N	$k_* = 0$		$k_* = 0.1$		$k_* = 0.5$		$k_* = 0.9$	
	LU	AMG	LU	AMG	LU	AMG	LU	AMG
9,539	28	350	9	179	8	171	7	169
37,507	28	445	9	212	8	205	8	202
148,739	28	545	9	247	8	236	8	234
592,387	28	597	9	271	8	265	8	265
$k^* = 1000$ N	$k_* = 0$		$k_* = 1$		$k_* = 10$		$k_* = 100$	
	LU	AMG	LU	AMG	LU	AMG	LU	AMG
9,539	3	75	3	75	3	75	3	75
37,507	3	94	3	94	3	94	3	94
148,739	3	116	3	116	3	116	3	116
592,387	3	139	3	139	3	139	3	139
$k^* = 10^8$ N	$k_* = 0$		$k_* = 1$		$k_* = 10^3$		$k_* = 10^6$	
	LU	AMG	LU	AMG	LU	AMG	LU	AMG
9,539	1	11	1	11	1	11	1	11
37,507	1	13	1	13	1	13	1	13
148,739	1	20	1	20	1	20	1	20
592,387	1	23	1	23	1	23	1	23

Here $\beta = \pi/4$ is the angle between Γ_1 and Γ_2 . In Figure 6.2 we show the computed streamlines of the magma and matrix velocity fields for this problem.

Table 6.4 presents the number of solver iterations for the LU and AMG preconditioners for different values of α . We observe very similar behaviour as we saw for the test in Section 6.1. The LU preconditioner is optimal and uniform. The AMG preconditioner again shows slight dependence on the problem size, and as α is increased the iteration count grows.

6.2.2. Traction-free problem. For the traction-free problem, instead of prescribing $\mathbf{u}_{\text{corner}}$, we prescribe the zero-traction boundary condition, $(\epsilon(\mathbf{u}) - p\mathbf{I} + \alpha\nabla \cdot \mathbf{u}\mathbf{I}) \cdot \mathbf{n} = 0$ on Γ_3 . Figure 6.3 shows the computed streamlines of the magma and matrix velocity fields for this problem.

The solver iteration counts for this problem with different levels of mesh refinement and for different values of α are presented in Table 6.5. As for the analytic corner flow problem of Section 6.2.1, the LU-based preconditioner is optimal and uniform. As expected, using the AMG-based preconditioner, the solver is not uniform

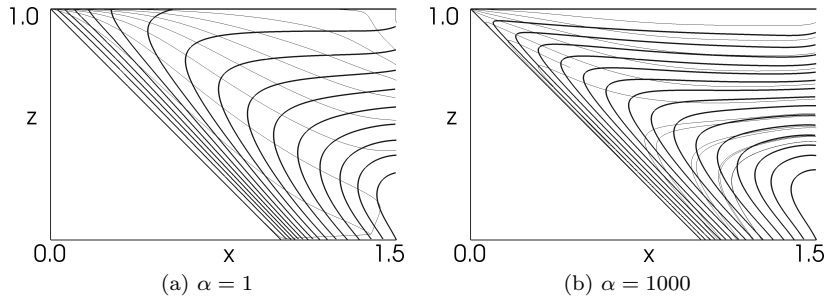


Fig. 6.2: Streamlines of the magma (light) and matrix (dark) velocity fields in the wedge of a two-dimensional subduction zone using the corner flow boundary condition on Γ_3 . The solution was computed on a mesh with 116176 elements.

Table 6.4: Number of iterations required for the corner flow problem using LU and AMG preconditioned MINRES for different levels of mesh refinement and varying α . For the $\alpha = 1000$ case, four applications of a Chebyshev smoother, with one symmetric Gauss-Seidel iteration for each application, was used.

N	$\alpha = 1$		$\alpha = 10$		$\alpha = 100$		$\alpha = 1000$	
	LU	AMG	LU	AMG	LU	AMG	LU	AMG*
34,138	26	69	30	140	30	367	28	572
133,777	26	75	29	151	27	390	27	669
526,719	24	81	29	171	26	446	27	758

with respect to α .

6.3. Magma dynamics problem in three dimensions. In the final case we test the solver for a three-dimensional problem that is geometrically representative of a subduction zone. We solve (2.17) and (2.18) on the domain Ω depicted in Figure 6.4. We set $L_x^t = 1.5$, $L_x^b = 0.5$, $L_y = 1$ and $L_z = 1$, and use unstructured meshes of tetrahedral cells. Again we set the permeability as $k = 0.9(1 + \tanh(-2r))$, with $r = \sqrt{x^2 + z^2}$, and the porosity $\phi = 0.01$.

As boundary conditions, we prescribe $\mathbf{u} = \mathbf{u}_{\text{slab}} = (1, 0.1, -1)/\sqrt{2}$ on Γ_1 , $\mathbf{u} = \mathbf{0}$ on Γ_2 , $(\boldsymbol{\epsilon}(\mathbf{u}) - p\mathbf{I} + \alpha\nabla \cdot \mathbf{u}\mathbf{I}) \cdot \mathbf{n} = 0$ on Γ_3 and $-k(\nabla p - \mathbf{e}_3) \cdot \mathbf{n} = 0$ on $\partial\Omega$. In Figure 6.5 we show computed vector plots of the matrix and magma velocities for $\alpha = 1$ and $\alpha = 1000$.

Table 6.6 shows the number of iterations needed for the AMG preconditioned MINRES method for the three-dimensional wedge problem. The LU preconditioned solver is not practical for this problem when using reasonable mesh resolutions. All cases have been computed in parallel using 16 processes. The computed examples span a range of problem sizes, and only relatively small changes in the iteration count are observed for changes in the number of degrees of freedom. Again, as α becomes larger, so too does the iteration count.

7. Conclusions. In this work we introduced and analysed an optimal preconditioner for a finite element discretisation of the simplified McKenzie equations for magma/mantle dynamics. Analysis of the preconditioner showed that the Schur com-

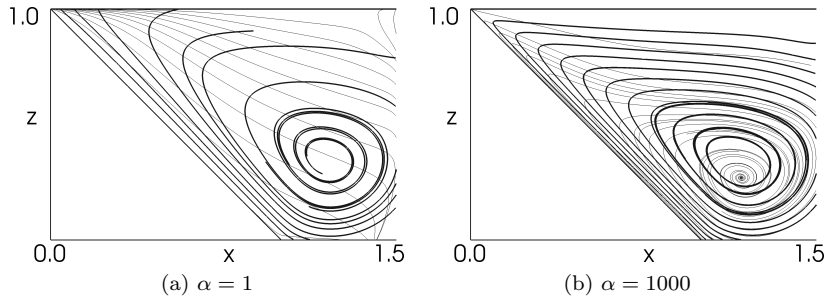


Fig. 6.3: Streamlines of the magma (light) and matrix (dark) velocity fields in the wedge of a 2D subduction zone using no stress boundary conditions on Γ_3 . The solution was computed on a mesh with 116176 elements.

Table 6.5: Number of iterations to reach a relative tolerance of 10^{-8} using LU and AMG preconditioned MINRES for different values of α for the no-stress test. For the $\alpha = 1000$ case, four applications of a Chebyshev smoother, with one symmetric Gauss-Seidel iteration for each application, was used.

N	$\alpha = 1$		$\alpha = 10$		$\alpha = 100$		$\alpha = 1000$	
	LU	AMG	LU	AMG	LU	AMG	LU	AMG*
34,138	24	65	29	143	27	375	25	626
133,777	23	73	27	159	27	424	24	718
526,719	23	80	26	175	27	475	24	798

plement of the block matrix arising from the finite element discretisation of the simplified McKenzie equations may be approximated by a pressure mass matrix plus a permeability matrix. The analysis was verified through numerical simulations on a unit square and two- and three-dimensional wedge flow problems inspired by subduction zones. For all computations we used P^2 - P^1 Taylor–Hood finite elements as they are inf-sup stable in the degenerate limit of vanishing permeability. Numerical tests demonstrated optimality of the solver. We observed that the multigrid version of the preconditioner was not uniform with respect to the bulk-to-shear-viscosity ratio α . As α is increased, the iteration count for the solver increases. We observe a similar behaviour as k^* increases.

The analysis and testing of an optimal block preconditioning method for magma/mantle dynamics presented in this work lays a basis for creating efficient and optimal simulation tools that will ultimately be put to use to study the genesis and transport of magma in plate-tectonic subduction zones. Optimality has been demonstrated, but some open questions remain regarding uniformity with respect to some model parameters.

Acknowledgements. We thank L. Alisic and J. F. Rudge for the many discussions held related to this paper. We also thank the reviewers M. Knepley, M. Spiegelman, C. Wilson and one that remained anonymous, whose comments helped improve this paper. The authors acknowledge the support of the Natural Environment Research Council under grants NE/I026995/1 and NE/I023929/1. Katz is furthermore

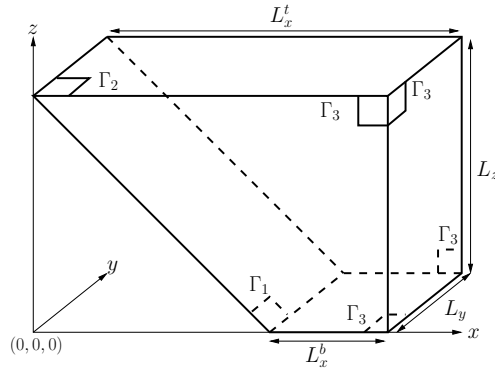


Fig. 6.4: Description of the wedge in a three-dimensional subduction zone.

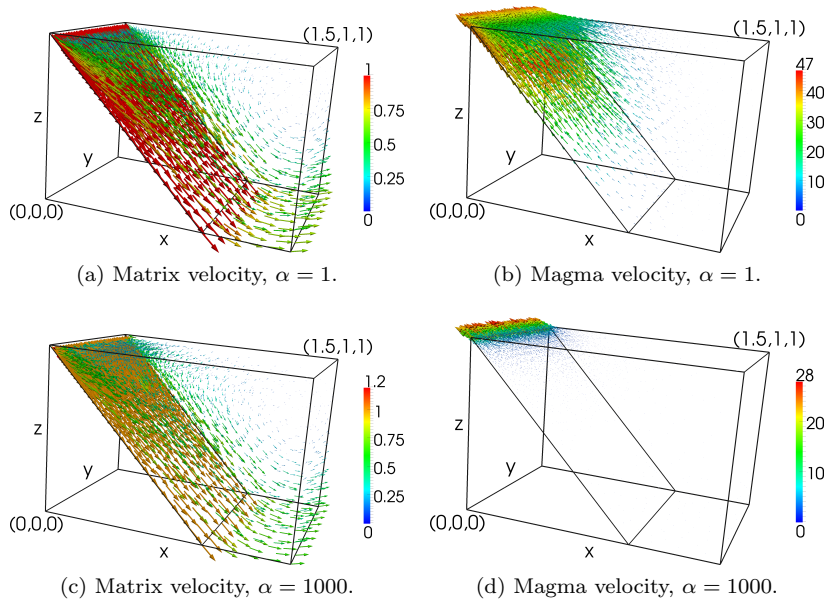


Fig. 6.5: Vector plots of the magma and matrix velocities in the wedge of a three-dimensional subduction zone for $\alpha = 1$ and $\alpha = 1000$ using the stress-free boundary conditions on Γ_3 .

grateful for the support of the Leverhulme Trust.

References.

- [1] E. Aharonov, J. A. Whitehead, P. B. Kelemen, and M. Spiegelman. Channeling instability of upwelling melt in the mantle. *J. Geophys. Res.*, 100:20433–20450, 1995.
- [2] M. S. Alnæs, A. Logg, K. B. Ølgaard, M. E. Rognes, and G. N. Wells. Unified Form Language: A domain-specific language for weak formulations of partial differential equations. *ACM Trans Math Software*, 40(2):9:1–9:37, 2014.

Table 6.6: Number of iterations required for AMG preconditioned MINRES for the three-dimensional subduction model for different levels of mesh refinement and different values of α . The number of degrees of freedom is denoted by N . For the $\alpha = 1000$ case, four applications of a Chebyshev smoother, with one symmetric Gauss-Seidel iteration for each application, was used. All tests were run using 16 MPI processes.

N	$\alpha = 1$	$\alpha = 10$	$\alpha = 100$	$\alpha = 1000$
88,500	42	127	363	654
400,690	44	122	355	692
1,821,991	43	122	367	732
8,124,691	41	120	355	775

- [3] D. N. Arnold, R. S. Falk, and R. Winther. Preconditioning in $H(\text{div})$ and applications. *Math. Comp.*, 66(218):957–984, 1997.
- [4] D. N. Arnold, R. S. Falk, and R. Winther. Multigrid in $H(\text{div})$ and $H(\text{curl})$. *Numer. Math.*, 85:197–217, 2000.
- [5] S. Balay, W. D. Gropp, L. C. McInnes, and B. F. Smith. Efficient management of parallelism in object oriented numerical software libraries. In E. Arge, A. M. Bruaset, and H. P. Langtangen, editors, *Modern Software Tools in Scientific Computing*, pages 163–202. Birkhäuser Press, 1997.
- [6] S. Balay, J. Brown, K. Buschelman, V. Eijkhout, W. D. Gropp, D. Kaushik, M. G. Knepley, L. C. McInnes, B. F. Smith, and H. Zhang. PETSc users manual. Technical Report ANL-95/11 - Revision 3.4, Argonne National Laboratory, 2013.
- [7] S. Balay, J. Brown, K. Buschelman, W. D. Gropp, D. Kaushik, M. G. Knepley, L. C. McInnes, B. F. Smith, and H. Zhang. PETSc Web page, 2014. URL <http://www.mcs.anl.gov/petsc>.
- [8] V. Barcilon and F. Richter. Nonlinear waves in compacting media. *J. Fluid Mech.*, 164:429–448, 1986.
- [9] G. K. Batchelor. *An Introduction to Fluid Dynamics*. Cambridge University Press, New York, 1967.
- [10] D. Bercovici and Y. Ricard. Energetics of a two-phase model of lithospheric damage, shear localization and plate-boundary formation. *Geophys. J. Int.*, 152: 581–596, 2003.
- [11] F. Brezzi and M. Fortin. *Mixed and Hybrid Finite Element Methods*. Springer-Verlag, New York, 1991.
- [12] J. Brown, M. G. Knepley, D. A. May, L. C. McInnes, and B. Smith. Composable linear solvers for multiphysics. In *2012 11th International Symposium on Parallel and Distributed Computing (ISPDC)*, pages 55–62, 2012. URL <http://dx.doi.org/10.1109/ISPDC.2012.16>.
- [13] H. C. Elman, D. J. Silvester, and A. J. Wathen. *Finite Elements and Fast Iterative Solvers*. Numerical Mathematics and Scientific Computation. Oxford University Press, 2005.
- [14] M. W. Gee, C. M. Siefert, J. J. Hu, R. S. Tuminaro, and M. G. Sala. *ML 5.0 smoothed aggregation users guide*. Sandia National Laboratories, 2006. Tech. Rep. SAND2006-2649.
- [15] A. Ghods and J. Arkani-Hamed. Melt migration beneath mid-ocean ridges. *Geophys. J. Int.*, 140:687–697, 2000.

- [16] P. P. Grinevich and M. A. Olshanskii. An iterative method for the Stokes-type problem with variable viscosity. *SIAM J. Sci. Comput.*, 31:3939–3978, 2009.
- [17] V. E. Henson and U. M. Yang. BoomerAMG: A parallel algebraic multigrid solver and preconditioner. *Appl. Numer. Math.*, 41(1):155–177, 2002.
- [18] R. F. Katz. Magma dynamics with the enthalpy method: Benchmark solutions and magmatic focusing at mid-ocean ridges. *J. Petrol.*, 2008.
- [19] R. F. Katz and Y. Takei. Consequences of viscous anisotropy in a deforming, two-phase aggregate: Part 2. Numerical solutions of the full equations. *J. Fluid Mech.*, 734:456–485, 2013.
- [20] R. F. Katz, M. Spiegelman, and B. Holtzman. The dynamics of melt and shear localization in partially molten aggregates. *Nature*, 442:676–679, 2006.
- [21] R. F. Katz, M. G. Knepley, B. Smith, M. Spiegelman, and E. T. Coon. Numerical simulation of geodynamic processes with the portable extensible toolkit for scientific computation. *Phys. Earth Planet. In.*, 163:52–68, 2007.
- [22] T. Keller, D. A. May, and B. J. P. Kaus. Numerical modelling of magma dynamics coupled to tectonic deformation of lithosphere and crust. *Geophys. J. Int.*, 195:1406–1442, 2013.
- [23] T. V. Kolev and P. S. Vassilevski. Parallel auxiliary space amg solver for $H(\text{div})$ problems. *SIAM J. Sci. Comput.*, 34(6):A3079–A3098, 2012.
- [24] A. Logg and G. N. Wells. DOLFIN: Automated finite element computing. *ACM Trans. Math. Software*, 37(2):20:1–20:28, 2010.
- [25] A. Logg, K.-A. Mardal, and G. N. Wells, editors. *Automated Solution of Differential Equations by the Finite Element Method*, volume 84 of *Lecture Notes in Computational Science and Engineering*. Springer, 2012.
- [26] D. A. May and L. Moresi. Preconditioned iterative methods for stokes flow problems arising in computational geodynamics. *Phys. Earth Planet. In.*, 171:33–47, 2008.
- [27] D. McKenzie. The generation and compaction of partially molten rock. *J. Petrol.*, 25:713–765, 1984.
- [28] K. B. Ølgaard and G. N. Wells. Optimisations for quadrature representations of finite element tensors through automated code generation. *ACM Trans Math Software*, 37(1):8:1–8:23, 2010.
- [29] J. Pestana and A. J. Wathen. Natural preconditioners for saddle point systems. 2013. URL <http://eprints.maths.ox.ac.uk/1754>.
- [30] S. Rhebergen, R. F. Katz, G. N. Wells, and A. Wathen. Supporting material, 2013. URL <https://bitbucket.org/magma-dynamics/preconditioning>.
- [31] G. Schubert, D. Turcotte, and P. Olson. *Mantle Convection in the Earth and Planets*. Cambridge University Press, 2001.
- [32] D. Silvester and A. Wathen. Fast iterative solution of stabilised Stokes systems. Part II: Using general block preconditioners. *SIAM J. Numer. Anal.*, 31:1352–1367, 1994.
- [33] G. Simpson, M. Spiegelman, and M. I. Weinstein. A multiscale model of partial melts: 1. Effective equations. *J. Geophys. Res.*, 115, 2010.
- [34] G. Simpson, M. Spiegelman, and M. I. Weinstein. A multiscale model of partial melts: 2. Numerical results. *J. Geophys. Res.*, 115, 2010.
- [35] M. Spiegelman. Flow in deformable porous-media. Part 1. Simple analysis. *J. Fluid Mech.*, 247:17–28, 1993.
- [36] M. Spiegelman. Flow in deformable porous media. Part 2. Numerical analysis—The relationship between shock waves and solitary waves. *J. Fluid Mech.*, 247:

- 39–63, 1993.
- [37] Y. Takei and R. F. Katz. Consequences of viscous anisotropy in a deforming, two-phase aggregate: Part 1. Governing equations and linearised analysis. *J. Fluid Mech.*, 734:424–455, 2013.
- [38] P. E. van Keken, C. Currie, S. D. King, M. D. Behn, A. Cagnioncle, J. He, R. F. Katz, S.-C. Lin, E. M. Parmentier, M. Spiegelman, and K. Wang. A community benchmark for subduction zone modeling. *Phys. Earth Planet. In.*, 171:187–197, 2008.
- [39] C. R. Wilson, M. Spiegelman, and P. E. van Keken. TerraFERMA: the Transparent Finite Element Rapid Model Assembler for multi-physics problems in Earth sciences. 2014. URL <https://bytebucket.org/tferma/tferma/wiki/TFpaperGcubed.pdf>.